Available online at www.sciencedirect.com
ScienceDirect
Journal of Nuclear Materials 357 (2006) 221–233
journal of nuclear materials
www.elsevier.com/locate/jnucmat

Solubility of crystalline and metamict zircon: A thermodynamic analysis

Desmond Tromans *

Department of Materials Engineering, University of British Columbia, 309-6350 Stores Road, Vancouver, BC, Canada V6T 1Z4

Received 9 March 2006; accepted 1 June 2006

Abstract

Thermodynamic analyses are used to predict the aqueous solubility of crystalline and metamict zircon at 25 °C and 150 °C for encapsulation purposes. The effect of the metamict state on solubility is treated as being equivalent to an increase in chemical free energy due to the development of amorphism. Both crystalline and metamict zircon exhibit pH-dependent behavior with minimum solubility at pH ~5.4 and ~4 for temperatures of 25 °C and 150 °C, respectively. Dissolution behavior may be incongruent or congruent, depending on pH, temperature and degree of metamictization (amorphism). A conservative approach is taken to the estimation of long-term dissolution rates at pH 5.4 and 4, based on a worst case scenario, where dissolution falls under mass transport control in the liquid phase. With increasing amorphism, unleached ZrO_2 residue produced during incongruent leaching conditions must function as an effective dissolution barrier to maintain long-term low dissolution rates.

PACS: 81.05.Je; 82.60.−s; 82.60.He; 91.60.Hg

MSC: 74A15 Thermodynamics

1. Introduction

Zircon ($ZrSiO_4$) is a ubiquitous mineral occurring in small amounts throughout the earth's crust in igneous, metamorphic and sedimentary rocks [1] The crystal space group ($I4_1/amd$, tetragonal) is isostructural with $USiO_4$ and $ThSiO_4$ and is able to incorporate small amounts of U and Th in substitution for Zr in the crystal lattice [1]. The natural mineral often contains traces of the radionuclides ^{238}U, and ^{235}U, together with ^{232}Th, and the radiogenic decay products ^{207}Pb and ^{206}Pb. Total weight concentrations of U, Th and Pb are variable in natural zircons, with U > Th > Pb. Values of U may reach a few thousand ppm and Pb and may reach a few hundred ppm by weight [2]. The presence of radionuclides allows natural zircons to be used for geochronology age-dating via concordia diagrams based on the isotopic ratios $^{207}Pb/^{235}U$ and $^{206}Pb/^{238}U$ [2–5]. The use of zircon for geochronology purposes is clear evidence of its

* Tel.: +1 604 822 2378; fax: +1 604 822 3619.
E-mail address: des@cmpe.ubc.ca

0022-3115/$ - see front matter
doi:10.1016/j.jnucmat.2006.06.012

durability over geological time and has led to the suggestion, notably by Weber et al. [6] and Ewing [7], that zircon ceramics may be candidate materials for the encapsulation and immobilization of radioactive wastes where radioactive actinides substitute for Zr in the crystal lattice.

Decay of the radionuclides in natural zircon occurs by emission of α-particles with high energies, *e.g.* 4.08 Mev, 4.268 MeV, 4.681 MeV for ^{232}Th, ^{238}U, and ^{235}U, respectively [8]. Dissipation of the particle energy causes damage in the crystal lattice along the track (10–20 μm) of the particle. via formation of point defects. However, the major damage is caused by recoil of the heavier α-emitting nucleus which produces smaller tracks (~10–40 nm) of locally disordered material [9–11]. Numerous emission events occurring over long periods of time develop more distorted crystalline regions and render increasing regions of the crystal lattice aperiodic, with no evidence of decomposition into ZrO_2 and SiO_2 products [9]. The naturally occurring radiation-induced damage process leading to aperiodicity (amorphism) in minerals such as zircon is known as metamictization and a mineral whose crystallinity has been damaged in this manner is known as a metamict [1]. The development of aperiodicity is readily detected by X-ray diffraction techniques via a decrease in peak intensity and broadening of X-ray lines [9,12], and changes in nuclear magnetic resonance spectra [10]. Deleterious side effects of metamictization are a decrease in density accompanied by localized swelling and microcrack formation [7,9,12,13]. Also, experimental studies and observations indicate that the solubility of metamict zircon in aqueous systems is lower than the fully crystalline zircon [2,12,14,15]. Similar amorphism and damage effects are expected to result from α-emission during decay of actinides in zircon encapsulated nuclear wastes to produce what is in effect a synthetic metamict (*i.e.* an aperiodic zircon). Consequently, it is reasonable to expect that natural and synthetic zircon metamicts, with similar degrees of amorphism (metamictization), will exhibit similar solubility effects.

The ambient conditions of ground waters in nuclear waste repositories are likely to be near neutral, with low ionic strength and temperatures < 160 °C [6,7], although temperatures up to 200 °C may occur [2]. There is a dearth of information on solubility behavior of crystalline and metamict zircons under these conditions, due to extremely low solubility and low dissolution rates, but such information is of utmost importance because nuclear waste repositories must function safely for tens of thousands of years. Tole [14] conducted limited experimental studies on crystalline and metamict zircon in pH 5.0 solutions between 25 °C and 80 °C and concluded that the metamict dissolves at a higher rate, with no measurable data obtainable for the crystalline zircon. In view of the difficulties encountered with measurement of corrosion rates at low temperatures, an alternative approach is to use thermodynamics to examine the likely solubility behavior of crystalline and amorphous (metamict) zircon. Tole [14] and Liermann et al. [5] introduced thermodynamic data into estimations of zircon solubility but were limited by incomplete data, particularly at temperatures higher than 25 °C. Leturcq et al. [16] also introduced thermodynamic calculations into a solubility study on Zr-based ceramic materials but did not include either zircons or metamicts.

The present study uses a complete and consistent set of thermodynamic data for all solid and aqueous species considered in order to construct pH-dependent solubility curves for zircon at 25 °C and 150 °C. The influence of amorphism (aperiodicity) on solubility is examined by treating it as an increase in the chemical free energy in the same manner as a previous study on the influence of amorphism on solubility of oxide films [17]. This approach establishes the likely conditions for congruent dissolution and the preferential leaching of oxide components (incongruent dissolution), together with conservative estimates of maximum dissolution rates. No distinction is made between the solubility of a natural and a synthetic metamict because amorphism occurs in both situations.

2. Thermodynamic data

Standard conventions were applied in the use of thermodynamic data, where the activity of a pure solid phase is equal to unity and the activity of water (liquid) is taken to be unity. Unit activity of a soluble species corresponds to a hypothetical one molal solution (1 mol solute per kg H_2O) referenced to infinite dilution. All solid and aqueous species considered in the analyses are listed in Table 1, together with their standard chemical free energies of formation ΔG_f° at 25 °C and 150 °C. The origins of the thermodynamic data, together with calculation procedures, are discussed in the following sections.

Table 1
Thermodynamic data

Species	Phase	ΔG_f°, kJ mol^{-1}		Data sources
		25 °C	150 °C	
SiO_2, quartz	(s)	−856.444	−833.582	Barin and Platzki [18]
ZrO_2, baddeleyite	(s)	−1039.724	−1015.603	Barin and Platzki [18]
$ZrSiO_4$, zircon	(s)	−1915.973	−1867.923	Barin and Platzki [18] Newton and Manning [20]
H_4SiO_4	(aq)	−1309.385	−1247.117	Rimstidt [23]
$H_3SiO_4^-$	(aq)	−1253.332	−1175.017	Busey and Mesmer [24]
$H_2SiO_4^{2-}$	(aq)	−1174.779	−1081.821	Busey and Mesmer [24]
Zr^{4+}	(aq)	−557.602	−528.964	Shock et al. [25]
$ZrOH^{3+}$	(aq)	−796.634	−760.724	Shock et al. [25]
ZrO^{2+}	(aq)	−784.918	−755.985	Shock et al. [25]
$HZrO_2^+$	(aq)	−1002.905	−950.784	Shock et al. [25]
$(ZrO_2)_{aq}$	(aq)	−976.546	−925.598	Shock et al. [25]
$HZrO_3^-$	(aq)	−1177.796	−1102.228	Shock et al. [25]
H^+	(aq)	0	0	Roine [28]
H_2O	(l)	−237.141	−217.468	Roine [28]

2.1. Solid species

Solid species considered were SiO_2 (quartz), ZrO_2 (baddeleyite) and $ZrSiO_4$ (zircon). Their ΔG_f° values at 25 °C and 150 °C were obtained from Barin and Platzki [18]. Values for SiO_2 and ZrO_2 were taken as listed but all $ZrSiO_4$ values were considered to contain a consistent error of −6.648 kJ mol^{-1} (*i.e.* should be more negative) and were corrected by this amount. The correction follows from two considerations. First, solid zircon decomposes into SiO_2 (cristobalite) and ZrO_2 (tetragonal) at 1676 °C [19] and chemical equilibrium requires that the ΔG_f° value of zircon at this temperature equals the sum of the chemical free energies of the SiO_2 and ZrO_2 phases, whereas the Barin and Platzki [18] data show that it is larger (more positive) by +6.648 kJ mol^{-1}. The second consideration arises from the experimental studies of Newton and Manning [20] who showed that the experimental Gibbs free energy of formation of zircon from SiO_2 (quartz) and ZrO_2 (baddeleyite) at 25 °C is -19.3 ± 1.16 kJ mol^{-1}, whereas the Barin and Platzki [18] data give a value of − 13.158 kJ mol^{-1} (*i.e.* too high by $+6.142 \pm 1.16$ kJ mol^{-1}).

2.2. Aqueous species

Aqueous Si and Zr species exist only in the +IV oxidation state in the domain of water stability so that chemical equilibria do not involve changes in oxidation state and may be represented by chemical reactions of the general thermodynamic form

$$aA + bB + hH^+ \cdots = cC + dD \cdots, \tag{1a}$$

$$(\Delta G^\circ)_{\text{reaction}} = -RT\ln(k) = -(2.30259)RT\log(k):$$

$$k = \left(\frac{[C]^c[D]^d \cdots}{[A]^a[B]^b[H^+]^h \cdots}\right), \tag{1b}$$

$$(\Delta G^\circ)_{\text{reaction}} = \sum(\Delta G_f^\circ)_{\text{products}} - \sum(\Delta G_f^\circ)_{\text{reactants}}, \tag{1c}$$

where A, B and H^+ are reactants; C and D are products; a, b, h, c, and d are integers; square brackets [ ] around species imply activities; k is the equilibrium constant; T is the temperature in degrees Kelvin (K); and R is the gas constant (8.31451 J K^{-1} mol^{-1}).

Note that H^+ may be a product (*i.e.* on the right hand side of Eq. (1a)), in which case h is negative, or it may not participate in the reaction and h becomes zero. By convention, the standard molal free energy of the H^+ ion in aqueous solutions is zero at all temperatures and pressures Also, $pH = -\log[H^+]$.

2.2.1. Si species

It is generally agreed that the equilibrium solubility of quartz in neutral and acidic solutions occurs via formation of the aqueous monomer species H_4SiO_4 of silicic acid [21,22]:

$$SiO_2 + 2H_2O = H_2SiO_4 \tag{2}$$

Rimstidt [23] has critically reviewed the equilibrium silica solubility data in water and developed a solubility function for the temperature range 0–300 °C based on experimental and published data

$$\log(m) = -1107.12(\pm 10.77)/T - 0.0254(\pm 0.0247), \quad (3)$$

where m is the molality of H_4SiO_4 (mol/kg H_2O) and T is degrees Kelvin (K).

The calculated molalities at 25 °C (298.15 K) and 150 °C (423.15 K) are sufficiently small, 1.8252×10^{-4} and 2.2815×10^{-3}, respectively, they may be taken to be equal to the activity (*i.e.* $m = [H_4SiO_4]$). Hence, knowing the ΔG_f° values of SiO_2 and H_2O, the ΔG_f° of H_4SiO_4 may be calculated via Eqs. (1b), (1c) and (2).

With increasing pH, hydrolysis of H_4SiO_4 occurs with development of the following equilibria:

$$H_4SiO_4 = H_3SiO_3^- + H^+; \quad k_{11} = \frac{[H_3SiO_3^-][H^+]}{[H_4SiO_4]} \quad (4)$$

$$H_4SiO_4 = H_2SiO_2^{2-} + 2H^+; \quad k_{12} = \frac{[H_2SiO_2^{2-}][H^+]^2}{[H_4SiO_4]} \quad (5)$$

Using potentiometric techniques and temperatures from 60 to 290 °C, Busey and Mesmer [24] showed that $\log k_{11}$ is −9.82 and −8.9 at 25 °C and 150 °C, respectively. Also, extrapolation of their k_{12} data to 25 °C, and interpolation at 150 °C, gave estimated $\log k_{12}$ values of −11.79 and −10.202, respectively, after correcting for activities of species. Hence, knowing ΔG_f° for H_4SiO_4 and H^+, the ΔG_f° values of $H_3SiO_3^-$ and $H_3SiO_2^{2-}$ may be calculated via Eqs. (1b), (1c), (4) and (5).

2.2.2. Zr species

Six aqueous Zr species were considered; Zr^{4+}, $ZrOH^{3+}$, ZrO^{2+}, $HZrO_2^+$, $(ZrO_2)_{aq}$, and $HZrO_3^-$. Their standard ΔG_f° values at 25 °C were obtained from Shock et al. [25]. Standard ΔG_f° values at 150 °C were computed from the 25 °C data using the revised Helgeson–Kirkham–Flowers (HKF) equation of state at a constant pressure of 1 bar. The effects of the pressure of water vapor at 150 °C (~4.7 bar) have negligible effect on the computations and are ignored. The form of the HKF equation is summarized in papers by Pokrovskii and Helgeson [26] and Dick et al. [27], and the required HKF parameters for the Zr species were obtained from Shock et al. [25]. The required dielectric constants of water for the HKF equation were 78.382 and 45.33 at 25 °C and 150 °C, respectively [28].

2.3. Chemical free energy of amorphous (aperiodic) phase

Previous studies by Tromans [17] and Tromans and Meech [29] have shown that estimates of the maximum difference in chemical free energy ΔG_{a-c} between a single solid oxide species in the fully amorphous (aperiodic) state (a) and the fully crystalline state (c) at any temperature T (K) may be obtained from a knowledge of the melting point T_m (K) and the enthalpy of fusion H_F (J mol^{-1})

$$(\Delta G_{a-c})_T = \left(\frac{H_F}{T_m}\right)(T_m - T), \quad (6)$$

If n polymorphic transitions occur between T and T_m, Eq. (6) is modified accordingly

$$(\Delta G_{a-c})_T = \sum_{n-1}^{n-n}\left(\frac{(H_\pi)_n}{(T_\pi)_n}\right)[(T_\pi)_n - T] + \left(\frac{H_F}{T_m}\right)(T_m - T), \quad (7)$$

where $(H_\pi)_n$ is the enthalpy of the nth polymorphous transition at the temperature $(T_\pi)_n$ and T is below the first transition temperature (*i.e.* $T < (T_\pi)_{n=1}$).

Calculated values of ΔG_{a-c} for SiO_2 and ZrO_2 at 25 °C and 150 °C, based on Eq. (7), are listed in Table 2, together with data sources for transition

Table 2
Estimated ΔG_{a-c} at 25 °C (298.1 K) and 150 °C (423.15 K)

Mineral	T_m (K)	H_F (kJ mol^{-1})	n	$(T_\pi)_n$ (K)	$(H_\pi)_n$ (kJ mol^{-1})	ΔG_{a-c} (kJ mol^{-1})		Data reference
						25 °C	150 °C	
SiO_2 (quartz)	1996	9.57	1	847	0.728	10.06	9.12	Barin and Platzki [18]
			2	1079	1.996			
ZrO_2 (baddeleyite)	2950	87.03	1	1478	5.941	83	78.8	Barin and Platzki [18]
$ZrSiO_4$ (zircon)	Incongruent melting at 1960 K		Decomposes into $ZrO_2 + SiO_2$ at 1949 K			~40?	~40?	Levin et al. [19] Ellsworth et al. [30]

temperatures and enthalpies. Similar calculations could not be done for $ZrSiO_4$, due to decomposition into its component oxides at 1676 °C (1949 K) followed by incongruent melting to give a mixture of solid and liquid phases at 1687 °C (1960 K) [19]. However, a tentative value of at least ~40 kJ mol^{-1} was assigned to the ΔG_{a-c} for zircon on the basis that is likely to be higher than SiO_2 and lower than ZrO_2, together with experimental observations of Ellsworth et al. [30] on a metamict zircon indicating that aperiodicity causes an enthalpy increase of $\Delta H_{a-c} = 59 \pm 3$ kJ mol^{-1} between the amorphous and crystalline state at room temperature.

Variations in the degree of amorphism /disorder may be treated conceptually by using fractionally different $\phi\Delta G_{a-c}$ values, where $0 < \phi < 1$ and ϕ equals zero for the fully crystalline state and is unity for the fully amorphous (disordered) state. Hence, when considering the fully amorphous oxide, its standard chemical free energy of formation $(\Delta G_f^\circ)_a$ is related to that of the fully crystalline state $(\Delta G_f^\circ)_c$ via the sum

$$(\Delta G_f^\circ)_a = (\Delta G_f^\circ)_c + \Delta G_{a-c}. \quad (8)$$

Similarly, the standard chemical free energy of the partially amorphous oxide is related to $(\Delta G_f^\circ)_c$ via the sum

$$\{(\Delta G_f^\circ)_a\}_{partial} = (\Delta G_f^\circ)_c + \phi\Delta G_{a-c}. \quad (9)$$

3. Solubility behavior

3.1. pH-dependent predominance of aqueous species

At any given temperature and pH, all soluble species of a given oxide–water system are present in larger or lesser degrees and affect the solubility of the oxide. Based on the chemical free energies of the species listed in Table 1, the relative distribution of soluble species in the SiO_2–H_2O system are shown in Fig. 1 and distributions for the ZrO_2–H_2O system are shown in Fig. 2. Distribution is expressed as the activity percentage of the specie of interest at a specific pH relative to the total summated activity of all species present at the same pH. Each figure shows the distributions at 25 °C and 150 °C.

Three reactions were considered in the SiO_2–H_2O system SiO_2

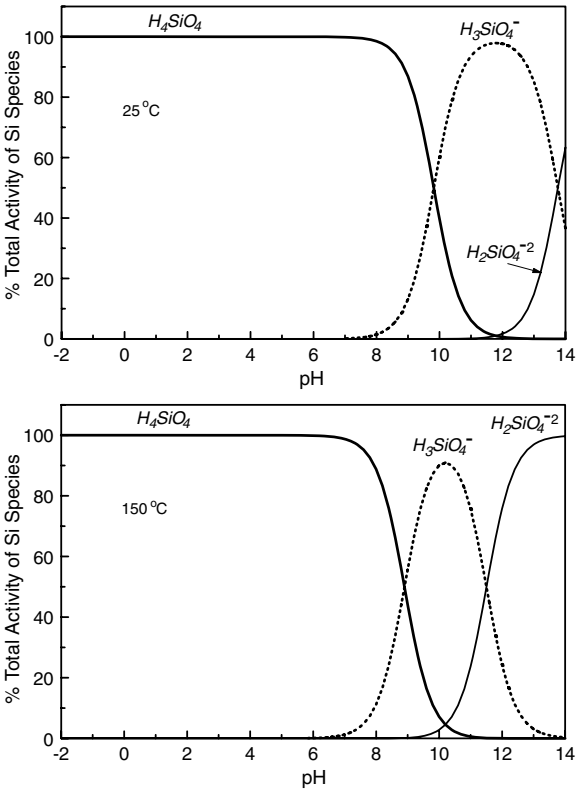

Fig. 1. Relative dominance of soluble Si species at 25 °C and 150 °C.

$$SiO_2 + 2H_2O = H_4SiO_4 \quad (10a)$$

$$SiO_2 + 2H_2O = H_3SiO_4^- + H^+ \quad (10b)$$

$$SiO_2 + 2H_2O = H_2SiO_4^{2-} + 2H^+ \quad (10c)$$

Six reactions were considered in the ZrO_2–H_2O system

$$ZrO_2 + 4H^+ = Zr^{4+} + 2H_2O \quad (11a)$$

$$ZrO_2 + 3H^+ = ZrOH^{3+} + H_2O \quad (11b)$$

$$ZrO_2 + 2H^+ = ZrO^{2+} + H_2O \quad (11c)$$

$$ZrO_2 + H^+ = HZrO_2^+ \quad (11d)$$

$$ZrO_2 = (ZrO_2)_{aq} \quad (11e)$$

$$ZrO_2 + H_2O = HZrO_3^- + H^+ \quad (11f)$$

3.2. Solubility behavior of SiO_2 (quartz) and ZrO_2 (baddeleyite)

The pH-dependent solubility behavior of quartz at 25 °C and 150 °C is shown in Fig. 3. The behavior

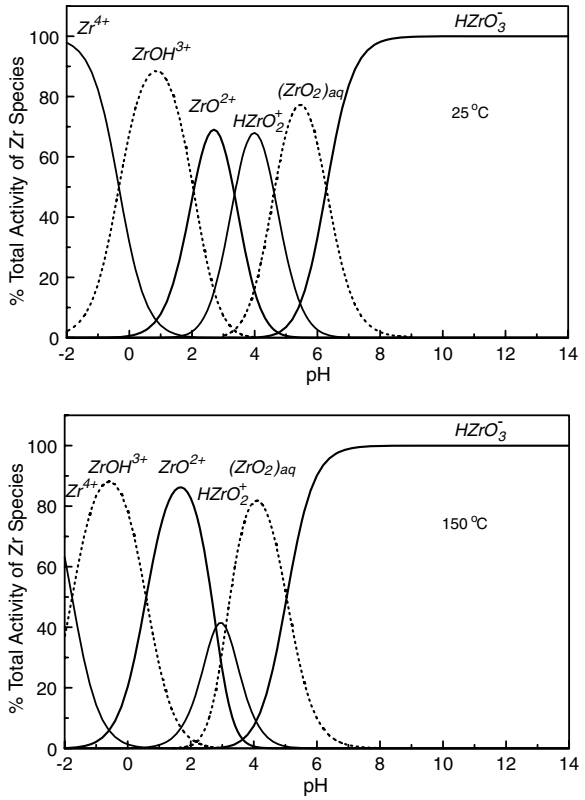

Fig. 2. Relative dominance of soluble Zr species at 25 °C and 150 °C.

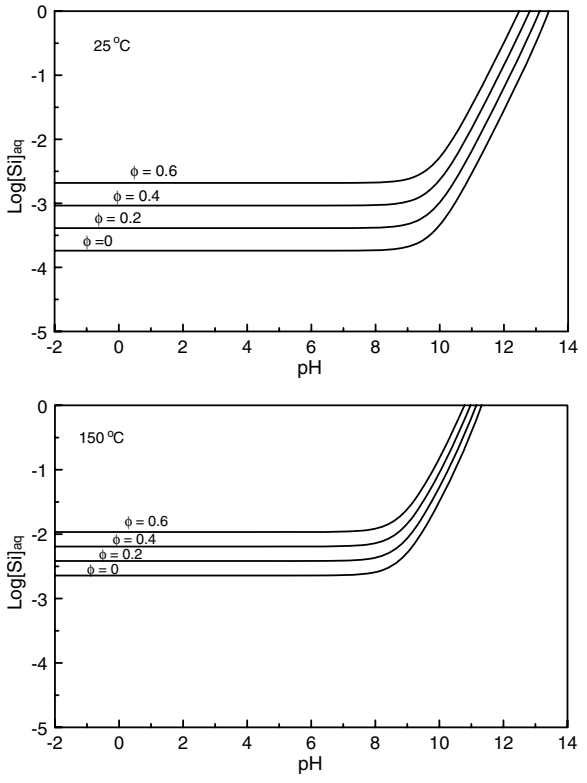

Fig. 3. Influence of ϕ-fraction on solubility behavior of SiO_2 (quartz) at 25 °C ($\Delta G_{a-c} = 10.06$ kJ mol^{-1}) and 150 °C ($\Delta G_{a-c} = 9.12$ kJ mol^{-1}), where $\phi = 0$ for the fully crystalline state.

of baddeleyite at the same temperatures is shown in Fig. 4. Solubility is expressed as the logarithm of the total summated activity of all soluble Si species ($Log[Si]_{aq}$) in Fig. 3 and soluble Zr species ($Log[Zr]_{aq}$) in Fig. 4. The behavior of the fully crystalline oxide is represented by the curve having a ϕ-fraction of zero (see Eq. (9)). The influence of increasing degrees of amorphism on the solubility is represented by curves with increasing ϕ-fractions of 0.2, 0.4 and 0.6. Examination of Figs. 3 and 4 shows the solubility of quartz in the near neutral pH range to be higher than that of baddeleyite, but the effects of increasing ϕ-fractions on quartz solubility are less pronounced than for baddeleyite. This follows directly from the much higher ΔG_{a-c} values for baddeleyite listed in Table 2.

In the near neutral pH-range, raising the temperature from 25 °C to 150 °C has little effect on the solubility of crystalline baddeleyite (Fig. 4), whereas there is a significant solubility increase for crystalline quartz (Fig. 3). Both minerals exhibit a small shift in the solubility minima to a lower pH, consistent with a decrease in the neutrality pH of water from 6.9985 to 5.825 [31]. The influence of ϕ-fraction on the increase in $Log[Si]_{aq}$ and $Log[Zr]_{aq}$ at 150 °C is less than at 25 °C, consistent with the fact that the increase in $Log[Si]_{aq}$ and $Log[Zr]_{aq}$ is $(\phi\Delta G_{a-c})/2.30259RT$ (see Eqs. (1b) and (9)).

Note that the solubility behavior of ZrO_2 at 25 °C was reported previously by the author [17], based on aqueous thermodynamic data compiled by Roine [28]. After reviewing that data and comparing it with the ΔG_f° data of Shock et al. [25], as used in the present study, it is considered that the Roine [28] compilation is in error, especially for the $HZrO_2^+$ and $HZrO_3^-$ species. Shock et al. [25] used hydrolysis constants to determine ΔG_f°, for the species, estimated the entropy S° of the ion, and then calculated the standard enthalpy of formation ΔH_f° from ΔG_f° and S°. In so doing a typographical error occurred in their reported ΔH_f° values for $HZrO_2^+$ and $HZrO_3^-$. The Roine [28] compilation used the ΔH_f° and S° values listed by Shock et al. [25] to compute ΔG_f°, thus introducing errors into their ΔG_f° values for $HZrO_2^+$ and $HZrO_3^-$.

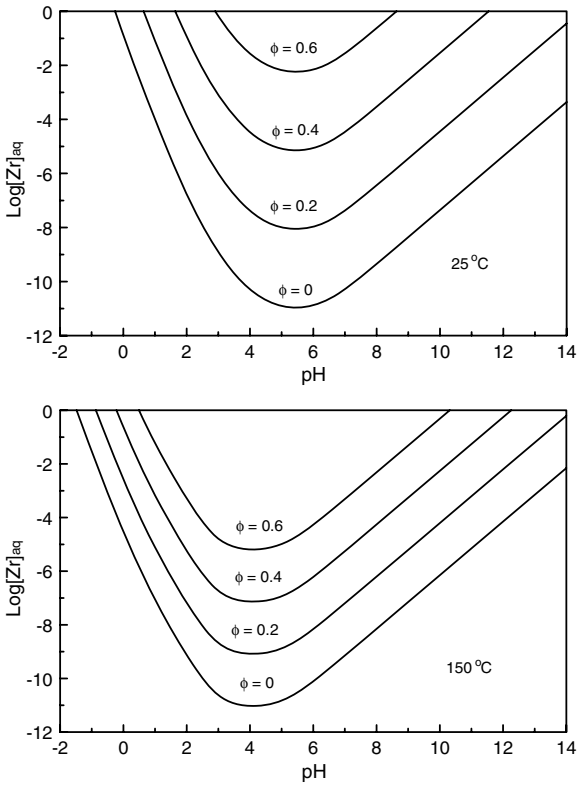

Fig. 4. Influence of ϕ-fraction on solubility behavior of ZrO_2 (baddeleyite) at 25 °C ($\Delta G_{a-c} = 83$ kJ mol^{-1}) and 150 °C ($\Delta G_{a-c} = 78.8$ kJ mol^{-1}), where $\phi = 0$ for the fully crystalline state.

3.3. Solubility behavior of $ZrSiO_4$ (zircon)

While the solubility of zircon will be influenced by the behavior of its component oxides shown in Figs. 3 and 4, overall behavior will be more complex because both congruent and incongruent dissolution of $[Si]_{aq}$ and $[Zr]_{aq}$ species must be considered. Reaction equations governing these processes are listed in Appendix A.

The influence of amorphism on the pH-dependent solubility of metamict zircon was assessed by conducting calculations for two $\phi\Delta G_{a-c}$ values of 18 kJ mol^{-1} and 36 kJ mol^{-1}. It was not possible to assign specific ϕ-fractions to the different metamict states because of uncertainty in the ΔG_{a-c} for zircon (see Table 2). For incongruent dissolution of the metamict, the unleached residue (either ZrO_2 or SiO_2) was treated as being disordered and the sum of the $\phi\Delta G_{a-c}$ values of the residues, $(\phi\Delta G_{a-c})_{ZrO_2} + (\phi\Delta G_{a-c})_{SiO_2}$ was set equal to the $\phi\Delta G_{a-c}$ value of the metamict zircon. The ratio $(\phi\Delta G_{a-c})_{ZrO_2}/(\phi\Delta G_{a-c})_{SiO_2}$ was approximated to the ratio $(\Delta G_{a-c})_{ZrO_2}/(\Delta G_{a-c})_{SiO_2}$ of the fully amorphous ZrO_2 and SiO_2 phases. From Table 2, this ratio is ~8:1. Consequently, a $\phi\Delta G_{a-c}$ value of 18 kJ mol^{-1} for metamict zircon, leads to assigned values of 16 kJ mol^{-1} and 2 kJ mol^{-1} for $(\phi\Delta G_{a-c})_{ZrO_2}$ and $(\phi\Delta G_{a-c})_{SiO_2}$, respectively. Similarly, a $\phi\Delta G_{a-c}$ value of 36 kJ mol^{-1} for metamict zircon, leads to assigned values of 32 kJ mol^{-1} and 4 kJ mol^{-1} for $(\phi\Delta G_{a-c})_{ZrO_2}$ and $(\phi\Delta G_{a-c})_{SiO_2}$, respectively. For the fully crystalline zircon, the unleached residues are treated as being in the fully crystalline state (*i.e.* ϕ-fraction = 0).

3.3.1. Congruent dissolution of zircon

Based on Eqs. (A.1)–(A.18) in Appendix A, ideal congruent solubility curves at temperatures of 25 °C and 150 are shown in Fig. 5 for the fully crystalline state (0 kJ mol^{-1}) and metamict states corresponding to $\phi\Delta G_{a-c}$ values of 18 kJ mol^{-1} and 36 kJ mol^{-1}. In analogous manner to Figs. 3 and 4, congruent solubility is seen to increase with increasing amorphism and the curves tend to move towards a slightly lower pH at the higher temperature.

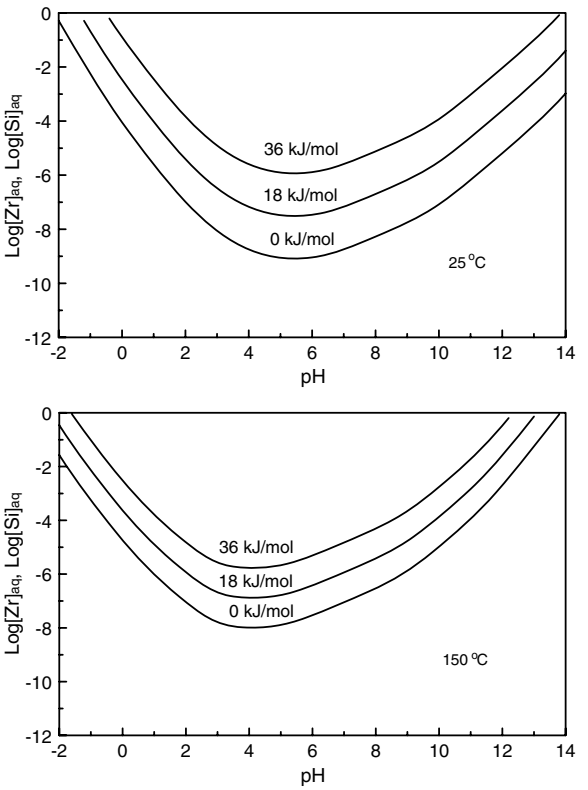

Fig. 5. Influence of increasing values of $\phi\Delta G_{a-c}$ on ideal congruent solubility behavior of crystalline zircon at 25 °C and 150 °C, where leaching of ZrO_2 and SiO_2 is ignored.

Comparison of Fig. 5 with Figs. 1 and 2 shows that the minimum solubility in all congruent dissolution curves occurs where the neutral soluble species H_4SiO_4 and $(ZrO_2)_{aq}$ are dominant. Furthermore, upon comparing Figs. 3 and 4 with Fig. 5, it is immediately apparent that congruent dissolution across the whole pH range is unlikely and preferential dissolution of SiO_2 or ZrO_2 must occur under some pH conditions.

3.3.2. Dissolution of crystalline zircon

The complete dissolution behavior of fully crystalline zircon at 25 °C and 150 °C is illustrated in Fig. 6, where both congruent and incongruent dissolution occur in different pH regimes. The dark shaded region represents the stability region of zircon and the lighter shaded regions show where preferential leaching is expected. The boundary line between the zircon and ZrO_2 regions shows where preferential leaching of SiO_2 occurs to leave unleached ZrO_2 residue according to Eqs. (A.19)–(A.21) in Appendix A. Similarly, the boundary line between the zircon and SiO_2 regions defines the conditions where ZrO_2 is leached to leave SiO_2 residue according to Eqs. (A.22)–(A.27) in Appendix A. The section of zircon stability line unbounded by either ZrO_2 or SiO_2 is the pH region of congruent dissolution and corresponds to a small segment of the idealized congruent curve at 0 kJ mol^{-1} in Fig. 5. Consequently, solubility behavior of crystalline zircon is dominated by incongruent dissolution behavior over a wide pH range, including the near neutral region. Raising the temperature decreases the stability region of zircon, displacing it to a lower pH, and reduces the pH range of congruent dissolution at 25 °C (−0.18 to 2.185 pH) to a range between −1.38 and 0.16 pH at 150 °C.

3.3.3. Dissolution of metamict zircon

The presence of the metamict (amorphous) state has a marked effect on zircon solubility. The complete solubility behavior at 25 °C and 150 °C is shown in Figs. 7 and 8 for $\phi\Delta G_{a-c}$ values of 18 kJ mol^{-1} and 36 kJ mol^{-1}, respectively. In Fig. 7, at 25 °C, the region of incongruent dissolu-

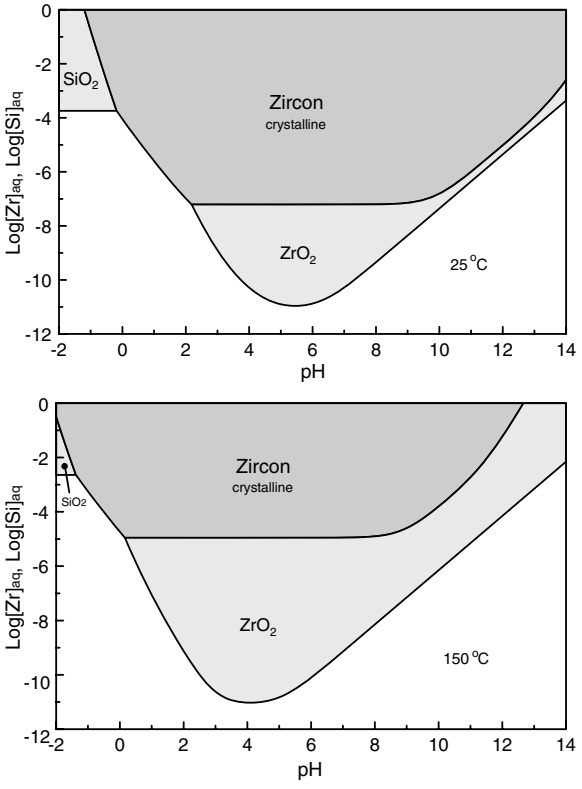

Fig. 6. Solubility behavior of crystalline zircon 25 °C and 150 °C when leaching is included in the analysis. Note dominance of incongruent solubility regions and diminished, pH-range of congruent solubility.

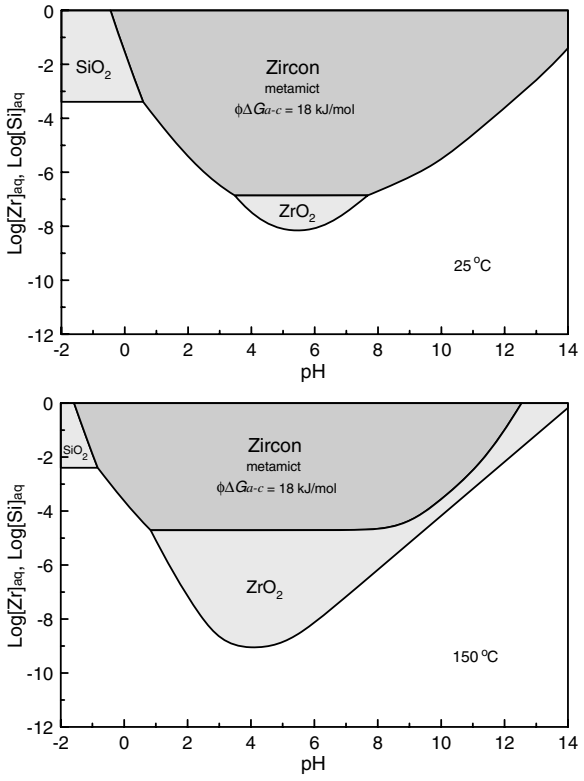

Fig. 7. Solubility behavior of a metamict (amorphous) zircon ($\phi\Delta G_{a-c} = 18$ kJ mol^{-1}) at 25 °C and 150 °C.

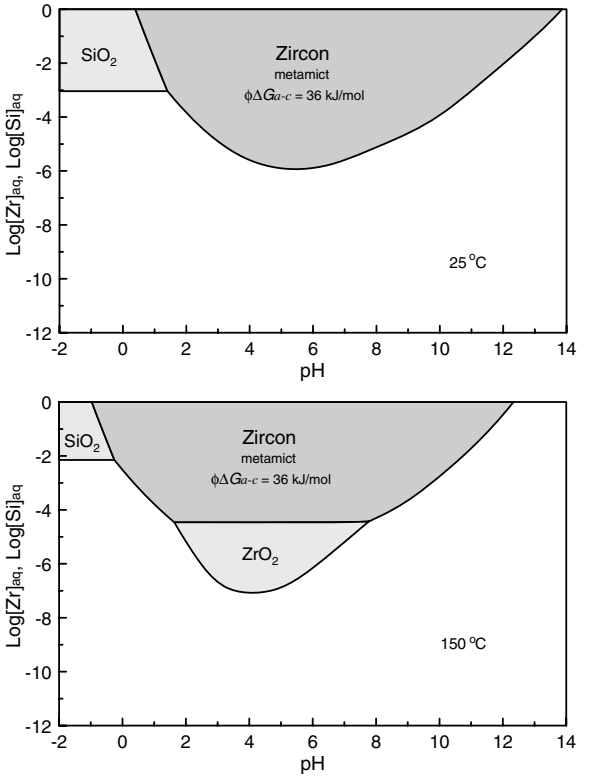

Fig. 8. Solubility behavior of a metamict (amorphous) zircon ($\phi\Delta G_{a-c} = 36$ kJ mol^{-1}) at 25 °C and 150 °C.

tion is decreased significantly, relative to Fig. 6 and congruent solubility behavior becomes much more dominant where it occurs in the pH ranges 0.58–3.48 pH and 7.78–14 pH. However, incongruent dissolution still prevails in the neutral pH and strongly acidic regions. Raising the temperature to 150 °C decreases the zircon stability region and restores the dominance of incongruent dissolution over a wide pH region, leaving a small pH range of congruent dissolution in the acid region between −0.83 and 0.84 pH.

Increasing $\phi\Delta G_{a-c}$ to 36 kJ mol^{-1} has a profound effect on the solubility of metamict zircon at 25 °C, as shown in Fig. 8. Solubility behavior is now dominated by congruent zircon dissolution from 1.41 to 14 pH. Incongruent dissolution is found only in the acid region at <1.41 pH. Raising the temperature to 150 °C again tends to decrease the zircon stability region and slightly displace it to towards a lower pH. However, more importantly, incongruent dissolution is restored in the near neutral pH range between 1.64 and 7.77, and congruent dissolution is confined to the pH ranges − 0.25 to 1.64 and >7.77 pH.

4. Discussion

4.1. General comments

Prediction of solubility behavior from chemical free energy data is dependent upon the accuracy of the data. Small changes in free energy values may affect the position of the solubility curves relative to the pH and Log[Si]$_{aq}$ or Log[Zr]$_{aq}$ axes. This is particularly true for oxides having very low solubility at ambient temperatures (e.g. ZrO_2) where it is more difficult to obtain reliable information. The data used in this study are considered to be the best available and sufficiently good to clearly demonstrate that the pH-dependent solubility behavior of crystalline and metamict zircon is quite complex. Dissolution may occur congruently or incongruently, and the pH regions within which such dissolution behaviors occur may change according to the temperature and degree of amorphism (*i.e.* $\phi\Delta G_{a-c}$) in the metamict state. Such complex behavior makes comparison between reported dissolution studies on zircon somewhat difficult, unless conducted under identical conditions, and probably justifies the description of zircon as being 'enigmatic in its resistance to chemical attack' [2].

Some experimental support for the current analyses arises from the work of Trocellier and Delmas [32] who subjected four natural zircons from Brazil and Madagascar to static dissolution tests in deionized water at 96 °C. After one month exposure, using mass spectrometry and spectrophotometry, they observed preferential leaching of Si with an approximately $\sim 1 \times 10^4$ times higher concentration of dissolved Si species ($5 \times 10^{-5} < (Si)_{aq} < 5 \times 10^{-4}$ mol L^{-1}) relative to the dissolved Zr species ($(Zr)_{aq} < 4 \times 10^{-9}$ mol L^{-1}). Referring to the crystalline zircon situation in Fig. 6, the maximum activity of soluble Si under incongruent dissolution (leaching) conditions is defined by the boundary line between the zircon and ZrO_2 regions, and the maximum activity of soluble Zr is defined by the lower ZrO_2 boundary line. At pH 7, Fig. 6 predicts a $[Si]_{aq}/[Zr]_{aq}$ activity ratio of $\sim 1.3 \times 10^3$ at 25 °C and $\sim 1.55 \times 10^4$ at 150 °C; giving encouragingly good agreement with the observed concentration ratio of $\sim 1 \times 10^4$ at 96 °C.

Tole [14] compared the dissolution behavior of crystalline zircon with that of a natural metamict zircon-type mineral (cyrtolite) containing 52.67 mol% ZrO_2, 29.81 mol% SiO_2 and 17.52 mol% of other oxides. After exposing both minerals to pH 5.0

solutions at 25, 60 and 80 °C for several hundred hours, no dissolution of the crystalline zircon was detected whereas dissolution of the metamict cyrtolite occurred, as measured by the presence of soluble Si species. While the composition of cyrtolite may affect the results to some degree, the enhanced dissolution of Si species from cyrtolite is consistent with that anticipated for a highly metamict state ($\phi\Delta G_{a-c} > 36$ kJ mol^{-1}) behaving in a congruent dissolution manner, similar to Fig. 8 at 25 °C. The absence of an unleached surface residue of ZrO_2 allows congruent dissolution to proceed unhindered, whereas unleached ZrO_2 residue that forms in the crystalline state at pH 5.0 (Fig. 6) could severely impede incongruent dissolution. Furthermore, the Zr species dissolving congruently with Si species in cyrtolite will exceed the solubility of crystalline baddeleyite (see Fig. 4) and precipitate in solution as unprotective ZrO_2. This will decrease the concentration of Zr species in solution to barely detectable or undetectable values, as reported by Tole [14].

The influence of complexing anions on zircon solubility has not been considered in the present study because such species are not expected to be present in nuclear waste repositories. However, it is interesting to note that hydrofluoric acid (HF) preferentially dissolves highly radiation damaged (metamict) regions of zircon much faster than undamaged regions at room temperature and has been used to isolate the least damaged (crystalline) regions in natural metamict zircon [15]. Figs. 6 and 8 at 25 °C are consistent with this behavior where the acidic stability region of the strongly metamict zircon (Fig. 8) is much reduced relative to the crystalline zircon (Fig. 6), leaving a larger unleached SiO_2 region which is readily dissolved in HF via the formation of aqueous SiF_6^{2-} and H_2SiF_6 complexes [33].

4.2. Conservative estimations of zircon dissolution rates

Thermodynamic analyses provide no direct information on the kinetics of dissolution, although an increase in the chemical free energy ($\phi\Delta G_{a-c}$) arising from amorphism in the metamict state could decrease the activation energy of surface controlled dissolution behavior in the manner discussed previously [29]. Also, Blum and Lasaga [34] have discussed the importance of surface controlled reactions on dissolution rates. However, a conservative approach to estimates of long-term repository behavior ought to be based on worst case scenarios involving the assumption of maximum dissolution rates, which in the final analysis are always mass transfer limited. While some workers such as Geisler et al. [2,12] have considered the role of mass transfer in the solid state, the fastest mass transfer occurs in the liquid phase. In the subsequent analysis, it is assumed that any flowing ground water systems around the depository are quiescent and the concentration of dissolved species in the bulk solution is negligible relative to the equilibrium concentration of dissolved species at the zircon surface. Furthermore, only liquid diffusion effects need be considered. Ion migration phenomena play no role because zircon dissolution is a chemical reaction and electrochemical potential gradients are absent.

The flux of dissolving species J across a plane in the solution normal to a reacting surface is given by the standard one dimensional diffusion equation corresponding to Fick's first law [35]:

$$J = -D(\partial c/\partial x),\ \text{mol m}^{-2}\,\text{s}^{-1}, \tag{12}$$

where D is the diffusion coefficient (m^2 s^{-1}), c is the concentration of species (mol m^{-3}), x (m) is the distance from the surface measured in the direction of diffusion, and $\partial c/\partial x$ is the concentration gradient.

Under steady state mass transfer controlled dissolution conditions most of the concentration changes occur in a liquid diffusion layer of thickness δ (m), through which the concentration decreases approximately linearly from c_s at the dissolving surface to c_b in the bulk solution [36,37]. Hence, Eq. (12) becomes

$$J = D(c_s - c_b)/\delta = (Dc_s)/\delta \quad \text{as } c_b \to 0,\ \text{mol m}^{-2}\,\text{s}^{-1}, \tag{13}$$

where c_s is the equilibrium thermodynamic concentration.

After multiplying Eq. (13) by the molar volume M_v (m^3 mol^{-1}) of zircon, the rate of dissolution of material, R_d (m s^{-1}) from the surface is obtained

$$R_d = (M_v D c_s)/\delta,\ \text{m s}^{-1}. \tag{14}$$

Examination of Figs. 6–8 in the neutral pH region, where ground waters are likely to lie, shows that SiO_2 is preferentially leached in all cases, except in Fig. 8 at 25 °C where congruent dissolution occurs. Therefore, two sets of calculations are undertaken to provide upper and lower limits on R_d. In the first set, the equilibrium concentration of the more soluble Si species in the neutral pH region is equated with c_s in Eq. (13) to obtain an

Table 3
Mass transport-controlled dissolution rates under minimum solubility conditions*

Zircon (state)	$\phi\Delta G_{a-c}$ (kJ mol^{-1})	Temperature (°C)	D (m^2 s^{-1})	pH	$[Si]_{aq}$	c_s (mol m^{-3})	R_d (upper value)	
							m s^{-1}	mm (ka)$^{-1}$
Crystal	0	25	3.38×10^{-9}	5.4	6.19×10^{-8}	6.19×10^{-5}	3.29×10^{-14}	1.04
Metamict	18	25	3.38×10^{-9}	5.4	1.39×10^{-7}	1.39×10^{-4}	7.36×10^{-14}	2.32
Metamict	36	25	3.38×10^{-9}	5.4	1.18×10^{-6}	1.18×10^{-3}	6.26×10^{-13}	19.7
Crystal	0	150	2.35×10^{-8}	4.0	1.11×10^{-5}	1.11×10^{-2}	4.09×10^{-11}	1290
Metamict	18	150	2.35×10^{-8}	4.0	1.96×10^{-5}	1.96×10^{-2}	7.23×10^{-11}	2280
Metamict	36	150	2.35×10^{-8}	4.0	3.46×10^{-5}	3.46×10^{-2}	1.28×10^{-10}	4025
Zircon (state)	$\phi\Delta G_{a-c}$ (kJ mol^{-1})	Temperature (°C)	D (m^2 s^{-1})	pH	$[Zr]_{aq}$	c_s (mol m^{-3})	R_d (lower value)	
							m s^{-1}	mm (ka)$^{-1}$
Crystal	0	25	3.38×10^{-9}	5.4	1.11×10^{-11}	1.11×10^{-8}	5.88×10^{-18}	1.85×10^{-4}
Metamict	18	25	3.38×10^{-9}	5.4	7.04×10^{-9}	7.04×10^{-6}	3.74×10^{-15}	0.118
Metamict	36	25	3.38×10^{-9}	5.4	1.18×10^{-6}	1.18×10^{-3}	6.26×10^{-13}	19.7
Crystal	0	150	2.35×10^{-8}	4.0	9.53×10^{-12}	9.53×10^{-9}	3.51×10^{-17}	1.11×10^{-3}
Metamict	18	150	2.35×10^{-8}	4.0	8.99×10^{-10}	8.99×10^{-7}	3.32×10^{-15}	0.105
Metamict	36	150	2.35×10^{-8}	4.0	8.49×10^{-8}	8.49×10^{-5}	3.13×10^{-13}	9.88

* Based on Eqs. (14) and (15), with $M_v = 3.962\times10^{-5}$ m^3 and $\delta = 2.5\times10^{-4}$ m.

upper limit on R_d. For the second set, the equilibrium concentration of the less soluble Zr species is set equal to c_s, at the same pH as that for the Si species to provide the lower limit R_d. This is done because the unleached ZrO_2 residue may act as a barrier to continued leaching, causing its dissolution to become rate-controlling.

The calculations are conducted at pH values corresponding to the solubility minima, which are pH 5.4 at 25 °C and pH 4 at 150 °C. The equilibrium activities of the soluble species under these conditions are sufficiently small that activity coefficients approach unity and the activity becomes indistinguishable from molal concentration (mol per kg H_2O), which is very similar to the molar concentration (mol per L or mol per dm^3 of solution). Hence, $c_s \approx [\text{Si or Zr}]_{aq}\times10^3$ mol m^{-3} and Eq. (14) becomes

$$R_d = (M_v D[\text{Si or Zr}]_{aq}\times10^3)/\delta,\ \text{m s}^{-1} \quad (15)$$

For calculation purposes, interferometry studies indicate δ is of the order $\sim2.5\times10^{-4}$ m under quiescent conditions [36,38] and diffraction data show that M_v is 3.926×10^{-5} m^3 [39]. The diffusion coefficients of the dissolving species are assumed to be very similar to the temperature-dependent self diffusion coefficient of water obtained from viscosity behavior by Tromans [40]

$$D = A\exp(-\Delta H_D/RT),\ \text{m}^2\text{s}^{-1} \quad (16)$$

where $A = 1.363\times10^{-6}$ m^2 s^{-1}; $\Delta H_D = 14227 + 4.661\times10^{19}T^{-6.8132}$ J mol^{-1}; and T is the temperature (K).

Table 3 shows calculated upper and lower R_d values for the minimum solubility conditions in Figs. 7 and 8. The R_d values are expressed in units of m s^{-1} and mm (ka)$^{-1}$ (*i.e.* mm per thousand years). It is very clear from the results that increasing amounts of amorphism, represented by $\phi\Delta G_{a-c}$, have a deleterious effect on dissolution behavior of metamict zircon by markedly increasing R_d rates based on soluble Si species. It is equally clear that it is important for the unleached ZrO_2 to act as an effective dissolution barrier because of its significantly lower R_d values, otherwise radiation damaged (metamict) zircon may prove to be unsuitable as a long-term encapsulation and immobilization material for radioactive wastes, unless the radioactive loading is maintained at very small levels.

Other important considerations relating to the use of zircon for storage of radioactive wastes is the pH of ground waters around the repository. Figs. 6–8 clearly show that minimum solubility occurs in the pH range 4–5.4. Significant movement of pH outside this range will adversely affect long-term dissolution behavior.

5. Conclusion

The solubility behavior of crystalline and metamict zircon is pH-dependent with minimum solubility occurring in the near neutral pH range of 4–5.4. Dissolution behavior is complex and may occur congruently or incongruently, depending upon temperature, pH and degree of metamictization

(amorphism). Increasing degrees of metamictization markedly diminish the long-term dissolution resistance of zircon, as evidenced from estimated thermodynamic solubility curves and calculations of conservative dissolution rates based on mass transport controlled behavior in the liquid phase. Zircon ceramics for the encapsulation and immobilization of radioactive wastes should contain low concentrations of radioactive species to minimize the effects of radiation-induced metamictization (amorphism) on long-term solubility behavior.

Acknowledgements

Funding from the Natural Sciences and Engineering Research Council of Canada (NSERC) is gratefully acknowledged. Also, the author wishes to thank Professor Robin W. Grimes for bringing attention to the radioactive waste problem, and Professor J.A. Meech for his interest and encouragement.

Appendix A

A.1. Reaction equations for zircon

Evaluation of zircon solubility required three additional sets of equations to be considered based on congruent dissolution of $[Si]_{aq}$ and $[Zr]_{aq}$ species, incongruent dissolution involving preferential leaching of $[Si]_{aq}$ species, and incongruent dissolution leading to preferential dissolution of $[Zr]_{aq}$ species. All dissolution processes are treated as stoichiometric reactions.

A.1.1. Congruent dissolution

Eighteen equations are required for a congruent dissolution

$$4H^+ + ZrSiO_4 = Zr^{4+} + H_4SiO_4 \quad (A.1)$$

$$3H^+ + ZrSiO_4 = Zr^{4+} + H_3SiO_4^- \quad (A.2)$$

$$2H^+ + ZrSiO_4 = Zr^{4+} + H_2SiO_4^{2-} \quad (A.3)$$

$$H_2O + 3H^+ + ZrSiO_4 = ZrOH^{3+} + H_4SiO_4 \quad (A.4)$$

$$H_2O + 2H^+ + ZrSiO_4 = ZrOH^{3+} + H_3SiO_4^- \quad (A.5)$$

$$H_2O + H^+ + ZrSiO_4 = ZrOH^{3+} + H_2SiO_4^{2-} \quad (A.6)$$

$$H_2O + 2H^+ + ZrSiO_4 = H_4SiO_4 + ZrO^{2+} \quad (A.7)$$

$$H_2O + H^+ + ZrSiO_4 = H_3SiO_4^- + ZrO^{2+} \quad (A.8)$$

$$H_2O + ZrSiO_4 = H_2SiO_4^{2-} + ZrO^{2+} \quad (A.9)$$

$$2H_2O + H^+ + ZrSiO_4 = H_4SiO_4 + HZrO_2^+ \quad (A.10)$$

$$2H_2O + ZrSiO_4 = H_3SiO_4^- + HZrO_2^+ \quad (A.11)$$

$$2H_2O + ZrSiO_4 = H_2SiO_4^{2-} + HZrO_2^+ + H^+ \quad (A.12)$$

$$2H_2O + ZrSiO_4 = H_4SiO_4 + ZrO_{2(aq)} \quad (A.13)$$

$$2H_2O + ZrSiO_4 = H_3SiO_4^- + ZrO_{2(aq)} + H^+ \quad (A.14)$$

$$2H_2O + ZrSiO_4 = H_2SiO_4^{2-} + ZrO_{2(aq)} + 2H^+ \quad (A.15)$$

$$3H_2O + ZrSiO_4 = H_4SiO_4 + HZrO_3^- + H^+ \quad (A.16)$$

$$3H_2O + ZrSiO_4 = H_3SiO_4^- + HZrO_3^- + 2H^+ \quad (A.17)$$

$$3H_2O + ZrSiO_4 = H_2SiO_4^{2-} + HZrO_3^- + 3H^+ \quad (A.18)$$

A.1.2. Incongruent dissolution: leaching of $[Si]_{aq}$ species

Three equations are required for leaching of the SiO_2 component

$$ZrSiO_4 + 2H_2O = H_4SiO_4 + ZrO_2 \quad (A.19)$$

$$ZrSiO_4 + 2H_2O = H_3SiO_4^- + H^+ + ZrO_2 \quad (A.20)$$

$$ZrSiO_4 + 2H_2O = H_2SiO_4^{2-} + 2H^+ + ZrO_2 \quad (A.21)$$

A.1.3. Incongruent dissolution with leaching of $[Zr]_{aq}$ species

Six equations are required for leaching of the ZrO_2 component

$$ZrSiO_4 + 4H^+ = Zr^{4+} + 2H_2O + SiO_2 \quad (A.22)$$

$$ZrSiO_4 + 3H^+ = ZrOH^{3+} + H_2O + SiO_2 \quad (A.23)$$

$$ZrSiO_4 + 2H^+ = ZrO^{2+} + H_2O + SiO_2 \quad (A.24)$$

$$ZrSiO_4 + H^+ = HZrO_2^+ + SiO_2 \quad (A.25)$$

$$ZrSiO_4 = ZrO_{2(aq)} + SiO_2 \quad (A.26)$$

$$ZrSiO_4 + H_2O = HZrO_3^- + H^+ + SiO_2 \quad (A.27)$$

References

[1] R.V. Gaines, H.C.W. Skinner, E.E. Foord, B. Mason, A. Rosenzweig, Dana's New Mineralogy, 8th Ed., John Wiley, New York, 1997.
[2] T. Geisler, R.T. Pidgeon, W. van Bronswijk, R. Kurtz, Chem. Geol. 191 (2002) 141.
[3] S.A. Bowring, D.H. Erwin, Y.G. Jin, M.W. Martin, K. Davidek, W. Wang, Science 280 (1998) 1039.
[4] M.D. Schmitz, S.A. Bowring, Chem. Geol. 172 (2000) 59.
[5] H-P. Liermann, C. Isachsen, U. Altenberger, R. Oberhänsli, Eur. J. Miner. 14 (2002) 61.
[6] W.J. Weber, R.C. Ewing, A. Meldrum, J. Nucl. Mater. 250 (1997) 147.
[7] R.C. Ewing, Proc. Natl. Acad. Sci. USA 96 (1999) 3432.
[8] R.L. Heath, in: R.C. Weast (Ed.), Handbook of Chemistry and Physics, 58th Ed., CRC Press, West Palm Beach, FL, 1978, p. B-270.

[9] T. Murakami, B.C. Chakoumakos, R.C. Ewing, G.R. Lumpkin, W.J. Weber, Am. Mineral. 76 (1991) 1510.
[10] I. Farnan, E.K.H. Salje, J. Appl. Phys. 89 (2001) 2084.
[11] R.C. Ewing, A. Meldrum, L. Wang, W.J. Weber, L.R. Corrales, Rev. Miner. Geochem. 53 (2003) 387.
[12] T. Geisler, A.A. Rashwan, M.K.W. Rahn, U. Poller, H. Zwingmann, R.T. Pidgeon, H. Schleicher, F. Tomaschek, Miner. Mag. 67 (2003) 485.
[13] J.M. Pruneda, T.D. Archer, E. Artacho, Phys. Rev. B 70 (2004) 104111.
[14] M.P. Tole, Geochim. Cosmochim. Acta 49 (1985) 453.
[15] D.W. Davis, T.E. Krogh, Chem. Geol. 172 (2001) 41.
[16] G. Leturcq, T. Advocat, K. Hart, G. Berger, J. Lacombe, A. Bonnetier, Am. Mineral. 86 (2001) 871.
[17] D. Tromans, J. Electrochem. Soc. 152 (2005) B460.
[18] I. Barin, G. Platzki, Thermochemical Data of Pure Substances, 3rd Ed., VCH, Weinheim, FRG, 1995.
[19] E.M. Levin, C.R. Robbins, H.F. McMurdie, Phase Diagrams for Ceramists 1969 Supplement, The American Ceramic Society, Columbus, OH, 1969, Fig. 2400, p. 110.
[20] R.C. Newton, C.E. Manning, J. Am. Ceram. Soc. 88 (2005) 1854.
[21] M.P. Verma, Geothermics 29 (2000) 323.
[22] J. Faimon, Aquatic Geochem. 11 (2005) 139.
[23] J.D. Rimstidt, Geochim. Cosmochim. Acta 61 (1997) 2553.
[24] R.H. Busey, R.E. Mesmer, Inorganic Chem. 16 (1977) 2444.
[25] E.L. Shock, D.C. Sassani, M. Willis, D.A. Sverjensky, Geochim. Cosmochim. Acta 61 (1997) 907.
[26] V.A. Pokrovskii, H.C. Helgeson, Chem. Geol. 137 (1997) 221.
[27] J.M. Dick, D.E. LaRowe, H.C. Helgeson, Biogeosci. Discuss. 2 (2005) 1515 (www.biogeosciences.net/bgd/2005-2-1515).
[28] A. Roine, HSC Chemistry for Windows, version 5.1, Chemical Reaction and Equilibrium Software with Extensive Thermochemical Database, Outokompu Research Oy, Pori, Finland, 2002.
[29] D. Tromans, J.A. Meech, Miner. Eng. 14 (2001) 1359.
[30] S. Ellsworth, A. Navrotsky, R. Ewing, Phys. Chem. Miner. 21 (1994) 140.
[31] C.M. Criss, J.W. Cobble, J. Am. Chem. Soc. 86 (1964) 5394.
[32] P. Trocellier, R. Delmas, Nucl. Instrum. and Meth. B 181 (2001) 408.
[33] Z. Galus, in: A.J. Bard, R. Parsons, J. Jordan (Eds.), Standard Potentials in Aqueous Solution, Marcel Dekker Inc., New York, 1985, p. 200.
[34] A. Blum, A. Lasaga, Nature 331 (1988) 431.
[35] R.C. Weast (Ed.), Handbook of Chemistry and Physics, 58th Ed., CRC Press, West Palm Beach, FL, 1978, p. F-62.
[36] K.J. Vetter, Electrochemical Kinetics, Academic Press, New York, 1967.
[37] D. Tromans, R-h. Sun, J. Electrochem. Soc. 138 (1991) 3235.
[38] Y. Awakura, Y. Kondo, J. Electrochem. Soc. 123 (1976) 1184.
[39] PDF-Powder Diffraction File # 06-0266, PCPDFWIN, JCPDS-International Center for Powder Diffraction Data, Swarthmore, PA, 1995.
[40] D. Tromans, Ind. Eng. Chem. Res. 39 (2000) 805.